Science Advances
AAAS

advances.sciencemag.org/cgi/content/full/5/1/eaav1851/DC1

Supplementary Materials for

Etching gas-sieving nanopores in single-layer graphene with an angstrom precision for high-performance gas mixture separation

J. Zhao, G. He, S. Huang, L. F. Villalobos, M. Dakhchoune, H. Bassas, K. V. Agrawal*

*Corresponding author. Email: kumar.agrawal@epfl.ch

Published 25 January 2019, *Sci. Adv.* **5**, eaav1851 (2019)
DOI: 10.1126/sciadv.aav1851

The PDF file includes:

References (*40–51*)

Note S1. High-resolution TEM (HRTEM)–based characterization of graphene.

An HRTEM study was carried out to understand the extent of amorphization in graphene after 6 s of plasma treatment (fig. S2). The image suggests that even after 6 s plasma treatment, there is no significant amorphization of graphene, although 2-5 nm sized nanopores are generated because of plasma-led etching. We note that for HRTEM sample preparation (see below), graphene was heated to 700 ^{o}C, and therefore we could not detect plasma generated sp^3-defects on graphene.

For HRTEM characterization, graphene was transferred onto a quantifoil TEM grid by a NPC film assisted transfer method. Briefly, a thin NPC film was formed on top of graphene via spin-coating of polymer solution and subsequent pyrolysis. Different with the conditions for graphene membrane preparation, 0.1 g poly(styrene-b-4-vinyl pyridine) and 0.05 g turanose were used in the polymer solution, and pyrolysis was done at 700 ^{o}C to obtain a NPC film with much higher porosity. One drop of solution was used for spin-coating to obtain ultrathin NPC film. The graphene/NPC film was transferred to a TEM grid. Aberration-corrected (Cs) HRTEM was performed using a double-corrected Titan Themis 60-300 (FEI) equipped with a Wein-type monochromator. HRTEM images were post-treated with Bandpass and Gaussian filters.

Note S2. Calculation of activation energy.

The permeance of gas through graphene nanopores, in the activated transport mode, can be expressed with the following equation:

$$P = C_o A exp(-\frac{E_{act}+E_{sur}}{RT}) \quad \text{(S1)}$$

where C_0 is the pore-density, A is the pre-exponential factor, E_{act} is the activation energy to translocate the pores, E_{sur} is the energy of adsorption on the graphene pore, R is the gas constant, T is the operation temperature.

By linear fitting of ln$P$ and 1/T, the apparent activation energy $E_{app-act} = E_{act} + E_{sur}$ can be obtained. Based on previous work (*40–42*), $E_{CO_2,sur}$= -17 kJ/mol, $E_{CH_4,sur}$= -13 kJ/mol, $E_{H_2,sur}$= -4 kJ/mol, $E_{He,sur}$= 0 kJ/mol, the E_{act} could be calculated by the equation $E_{act} = E_{act-app} - E_{sur}$.

Note S3. Estimation of the percentage of the nonselective nanopores in graphene.

The nanopores in graphene membrane can be roughly grouped into two categories: the large nanopores contributing to the effusive transport, and the molecular-selective pores contributing to the activated transport. The transmission coefficient for gas molecules (H_2, CH_4, C_3H_8 and SF_6) from a large nanopore (10^{-19} - 10^{-18} mol s^{-1} Pa^{-1}) is several orders of magnitude higher than that from a molecular-selective pore (< 10^{-22} mol s^{-1} Pa^{-1}).(*1*, *2*, *6*) Therefore, we can expect that the percentage of large pores in the graphene membranes is rather low, otherwise the gas selectivities will not be far above the corresponding Knudsen selectivities.
Typically, the H_2 and CH_4 permeances from the graphene membrane of can be written as

$$Permeance_{H_2} = C_e\, N_{e,H_2} + C_a\, N_{a,H_2} \quad \text{(S2)}$$

$$Permeance_{CH_4} = C_e\, N_{e,CH_4} + C_a\, N_{a,CH_4} \quad \text{(S3)}$$

where N_e is the permeation coefficient for the effusive transport, N_a is the permeation coefficient for the activated transport. C_e and C_a correspond to the density of pores contributing to the effusive and the activated transport, respectively. The gas selectivity α_{H_2/CH_4} can be written as

$$\alpha_{H_2/CH_4} = \frac{Permeance_{H_2}}{Permeance_{CH_4}} = \frac{C_e\, N_{e,H_2} + C_a\, N_{a,H_2}}{C_e\, N_{e,CH_4} + C_a\, N_{a,CH_4}} \quad \text{(S4)}$$

Rearranging above, we get

$$\alpha_{H_2/CH_4} = \left(\frac{N_{a,H_2}}{N_{a,CH_4}}\right)\left(\frac{1 + \frac{C_e}{C_a}\frac{N_{e,H_2}}{N_{a,H_2}}}{1 + \frac{C_e}{C_a}\frac{N_{e,CH_4}}{N_{a,CH_4}}}\right) \quad \text{(S5)}$$

Similarly, H_2/C_3H_8 and H_2/SF_6 selectivities can also be expressed as a function of the pore-density ratio.

$$\alpha_{H_2/C_3H_8} = \left(\frac{N_{a,H_2}}{N_{a,C_3H_8}}\right)\left(\frac{1 + \frac{C_e'}{C_a'}\frac{N_{e,H_2}}{N_{a,H_2}}}{1 + \frac{C_e'}{C_a'}\frac{N_{e,C_3H_8}}{N_{a,C_3H_8}}}\right) \quad \text{(S6)}$$

$$\alpha_{H_2/SF_6} = \left(\frac{N_{a,H_2}}{N_{a,SF_6}}\right)\left(\frac{1 + \frac{C_e''}{C_a''}\frac{N_{e,H_2}}{N_{a,H_2}}}{1 + \frac{C_e''}{C_a''}\frac{N_{e,SF_6}}{N_{a,SF_6}}}\right) \quad \text{(S7)}$$

For the effusive transport through a certain large pore, the permeation coefficient is proportional to $m^{-1/2}$, where m is the molecular weight of the gas. Since N_{e,H_2} is about 10^{-18} mol s^{-1} Pa^{-1},(*2*) the permeation coefficients for CH_4, C_3H_8 and SF_6 can be estimated as following: N_{e,CH_4} =3.54×10^{-19} mol s^{-1} Pa^{-1}, N_{e,C_3H_8} =2.13×10^{-19} mol s^{-1} Pa^{-1}, N_{e,SF_6} =1.17×10^{-19} mol s^{-1} Pa^{-1}. For the activated transport, N_{a,H_2} and N_{a,CH_4} are approximated to be 10^{-22} mol s^{-1} Pa^{-1} and 10^{-26} mol s^{-1} Pa^{-1}, respectively, based on the measurements by Bunch and co-workers.(*1*) Although the permeation coefficients of C_3H_8 and SF_6 from hydrogen-sieving pores haven't been reported in literatures, they should be lower than 10^{-26} mol s^{-1} Pa^{-1}. In any case, the variation of permeation coefficient lower than 10^{-26} mol s^{-1} Pa^{-1} has negligible influence on the final result of above analysis. Therefore, N_{a,SF_6} and N_{a,C_3H_8} are approximated as 10^{-26} mol s^{-1} Pa^{-1} in the following equations. By plugging the data into the equations S5-S7, we can get the correlations between pore density ratios and gas selectivities as following:

$$\frac{C_e}{C_a} = \left(\frac{\alpha_{H_2/CH_4} - 10^4}{10^8 - 3.54\times10^7 \alpha_{H_2/CH_4}}\right) \quad \text{(S8)}$$

$$\frac{C_e'}{C_a'} = \left(\frac{\alpha_{H_2/\,C_3H_8} - 10^4}{10^8 - 2.13\times10^7 \alpha_{H_2/\,C_3H_8}}\right) \quad \text{(S9)}$$

$$\frac{C_e''}{C_a''} = \left(\frac{\alpha_{H_2/SF_6} - 10^4}{10^8 - 1.17\times10^7 \alpha_{H_2/SF_6}}\right) \quad \text{(S10)}$$

Based on above, we can get the estimated percentage of the non-selective nanopores for different gas molecules in graphene (table S4 and table S8).

Note S4. Estimation of the defect density from Raman.

In the low-defect-density stage of graphene, the average distance between defects, L_d, can be calculated from the following relation: (*22*, *23*)

$$L_D^2(nm^2) = (1.8 \pm 0.5) \times 10^{-9}\, \lambda^4 (\frac{I_D}{I_G})^{-1} \quad \text{(S11)}$$

where λ is the Raman excitation wavelength (457 nm in our case).

In the high-defect-density stage, the relationship between I_D/I_G and L_d conforms to the following equation: (*22*, *23*)

$$\frac{I_D}{I_G} = D(\lambda) \times\ L_d^2 \quad \text{(S12)}$$

where $D(\lambda)$ can be obtained by imposing continuity between the two stages (~0.055 nm^{-2} in our case).

Figure S1 shows the correlation between L_d and I_D/I_G. The L_d value for graphene with intrinsic defects is about 47 nm, indicating a small density of defects in the as-synthesized CVD graphene. The defect density (number of defects per unit area), n_D, can be roughly estimated from L_d values from the following equation: (*23*)

$$n_D(cm^{-2}) = 10^{14}/(\pi L_d^2) \quad \text{(S13)}$$

The defect density of graphene membrane with intrinsic defects is estimated to be 1.5×10^{10} cm^{-2}, which increases by about 20 times to 3.0×10^{11} cm^{-2} after exposure to O_2 plasma for only 1 s, confirming the rapid formation of abundant nuclei during the plasma treatment. After further 1 s plasma exposure, the defect density continues to increase to 5.7×10^{11} cm^{-2}.

After exposing the 1 s plasma graphene to O_3 at 150 ^oC for 10 s, the I_D/I_G changed to 0.82±0.02, while I_{2D}/I_G decreased to 0.35±0.05. According the equation S12 and S13, the defect density can be estimated to be 2.1×10^{12} cm^{-2} (2.1 pores/100 nm^2).

Note S5. Measurement of the O_3 residence time.

After the startup of O_3 generator, it takes a certain time to generate O_3 steadily. The mixture of O_2/O_3 reaches the membrane module via flow connections, and as a result, there is a residence time for O_3 between the O_3 generator and the membrane. In order to ascertain the exact value of residence time, we connected O_3 generator with an O_3 analyzer (BMT964BT, BMT MESSTECHNIK) using the same length of connections and recorded the O_3 concentration. As shown in fig. S4, the O_3 concentration keeps at 0 g Nm^{-3} at first, and then shows a sharp increase beyond 35 s.

Note S6. Desorption of contaminants before permeation test.

Typically, atmospheric contaminants adsorb on the graphene lattice during the membrane fabrication steps (etching of Cu, rinsing, drying, etc.). As a result, the as-prepared membranes are often clogged, however, the contaminants can be easily desorbed by simply heating the membrane in an oven under a gas flow at 150 ºC for 30 min. For example, fig. S6A reveals the permeation data (H_2 and CH_4 permeances and the corresponding H_2/CH_4 selectivity) of the membrane M14 prepared by the 1 s plasma treatment. The as-synthesized membrane yielded lower than expected permeances at 30 ºC, attributing to the contaminant-led clogging. However, after a short heat-treatment at 150 ºC, the H_2 permeance at 30 ºC increased 4-fold from 56 GPU to 216 GPU, while the H_2/CH_4 selectivity also increased from 5.9 to 7.3. After removing the contaminants, the membrane performance remained stable for the duration of testing (60 hours, fig. S6B).

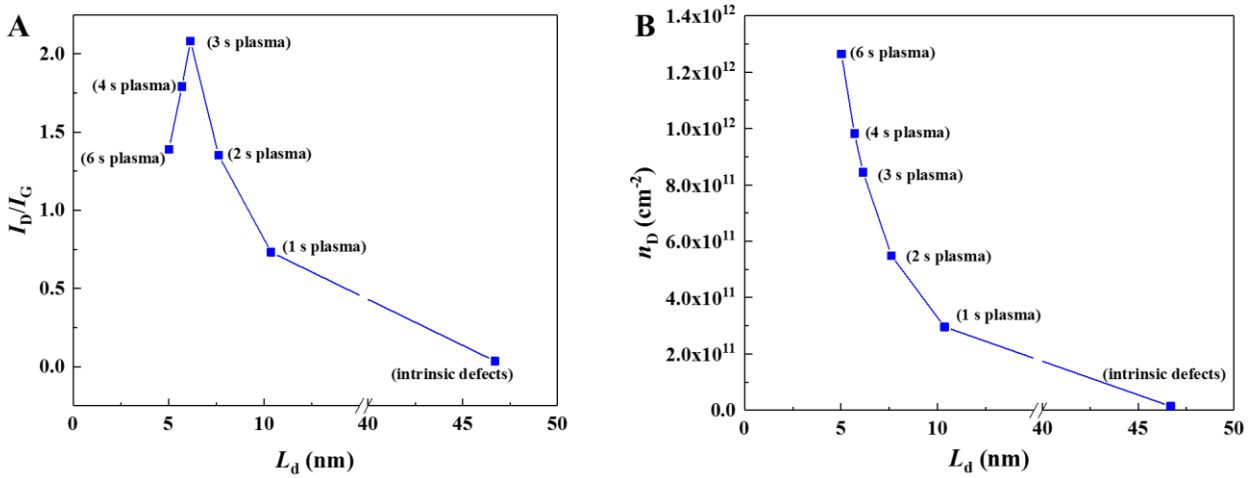

Fig. S1. The correlation between L_d, n_d, and I_D/I_G. (**A**) L_d~I_D/I_G, (**B**) L_d~n_d.

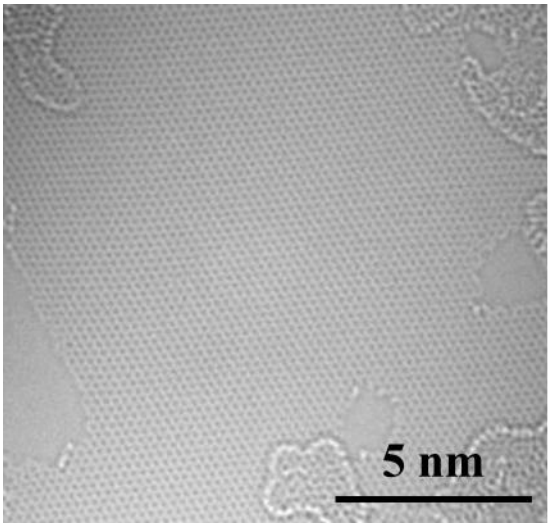

Fig. S2. HRTEM image of graphene after 6-s plasma treatment.

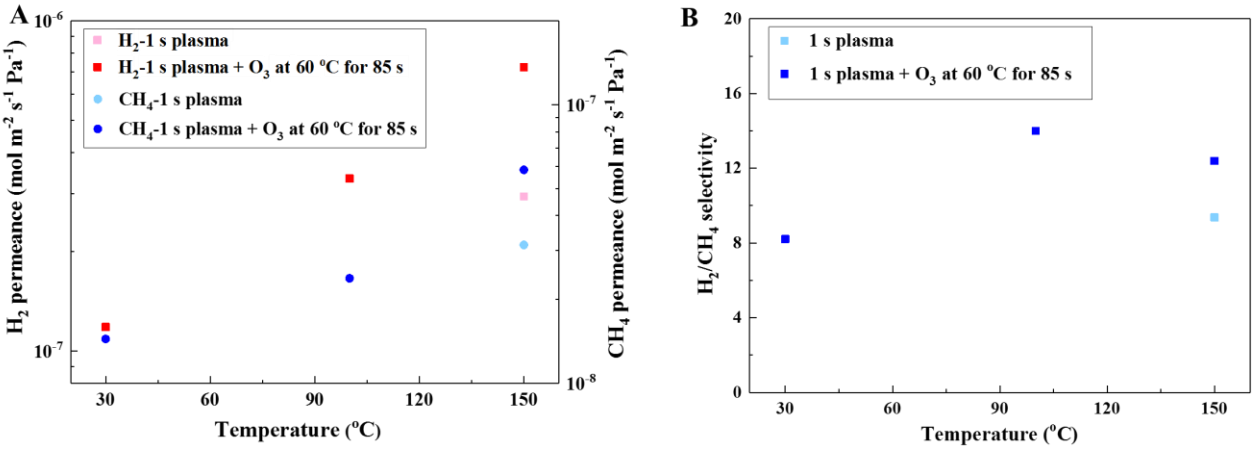

Fig. S3. Gas permeation performance of 1-s plasma-treated graphene M7 after 60°C O_3 treatment for 85 s. (**A**) H_2 and CH_4 permeance, (**B**) H_2/CH_4 selectivity.

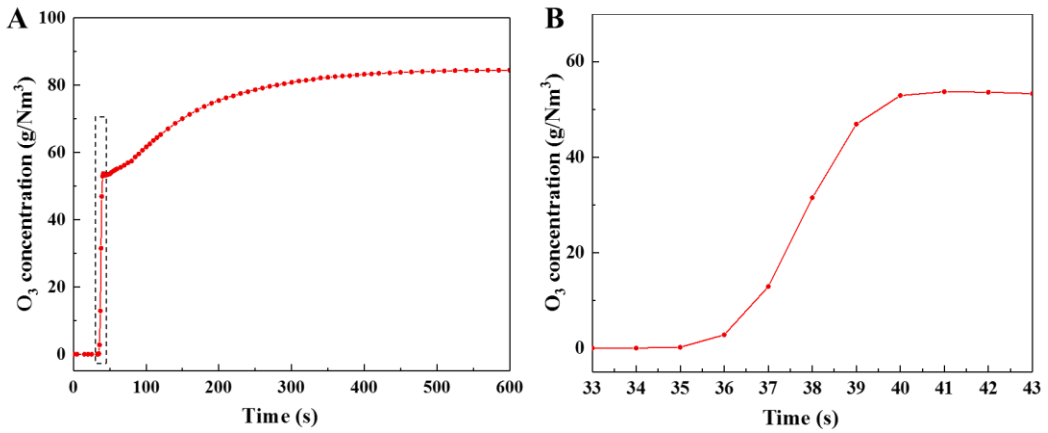

Fig. S4. The variation of O_3 concentration in membrane module. (B) is the zoomed version of the enclosed area in (A).

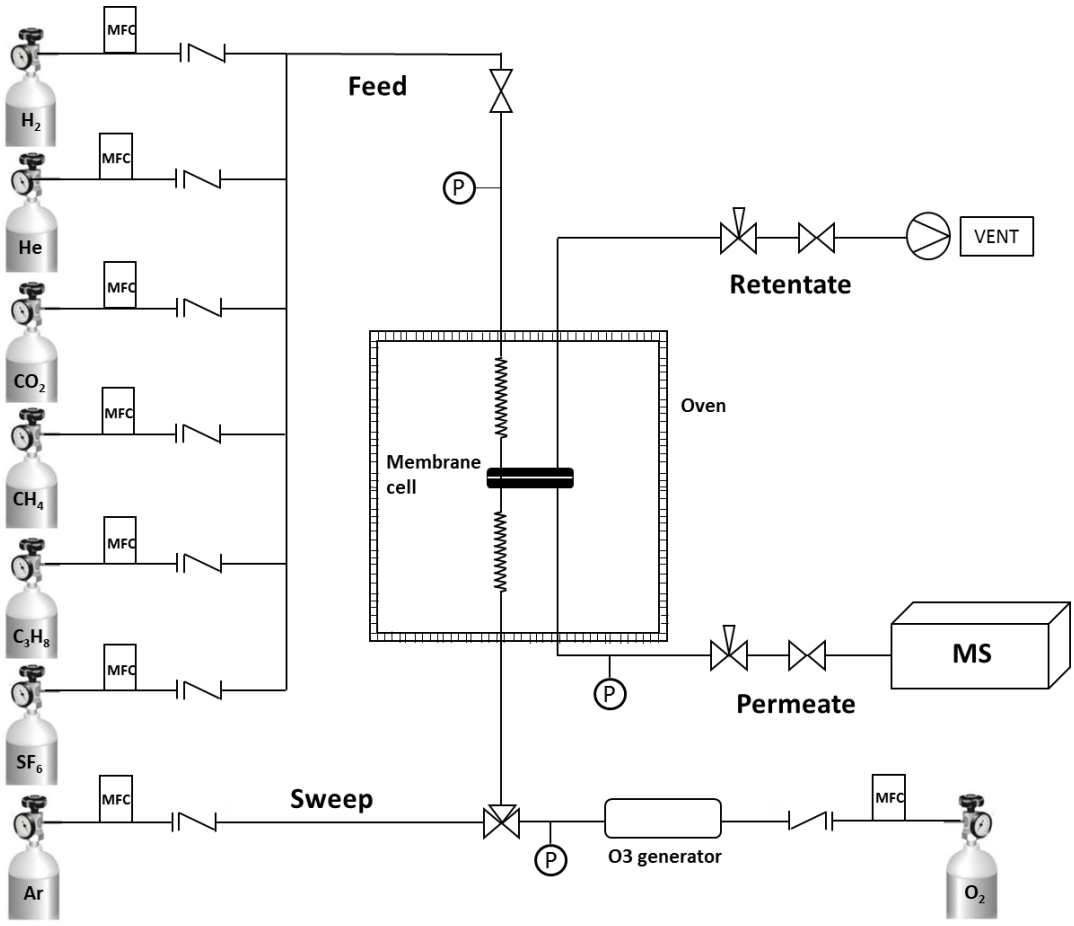

Fig. S5. Schematic of the setup for gas permeation test.

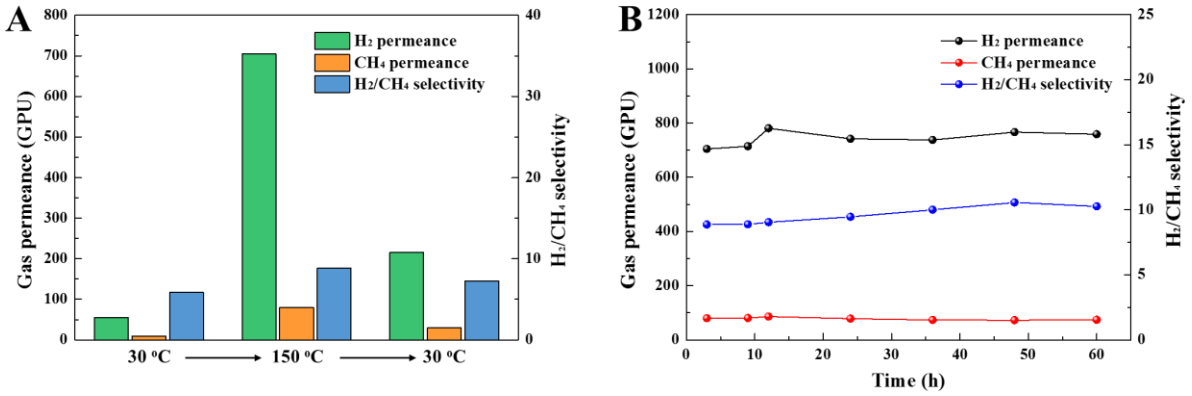

Fig. S6. Gas permeation performance of 1-s plasma-treated graphene M14. (**A**) Gas permeation performance before and after 150 ^{o}C treatment. (**B**) Long-term gas permeation performance at 150 ^{o}C.

Table S1. Gas permeance from M1 to M13 at 150°C.

Gas	Intrinsic-defects				1 s plasma							2 s plasma	
	M1	M2	M3	M4	M5	M6	M7	M8	M9	M10	M11	M12	M13
H_2	6.6×10^{-8}	5.5×10^{-8}	5.1×10^{-8}	9.1×10^{-8}	7.1×10^{-7}	3.5×10^{-7}	2.9×10^{-7}	2.5×10^{-7}	2.3×10^{-7}	2.4×10^{-7}	5.2×10^{-7}	9.2×10^{-7}	1.8×10^{-6}
He	8.2×10^{-8}	4.7×10^{-8}	3.4×10^{-8}	8.9×10^{-8}	4.6×10^{-7}	3.5×10^{-7}			2.1×10^{-7}				
CO_2	2.9×10^{-8}	1.5×10^{-8}	1.1×10^{-8}	2.5×10^{-8}	1.9×10^{-7}	1.2×10^{-7}			7.5×10^{-8}		1.4×10^{-7}	2.2×10^{-7}	5.0×10^{-7}
CH_4	4.9×10^{-9}	2.6×10^{-9}	3.2×10^{-9}	3.9×10^{-9}	8.4×10^{-8}	3.6×10^{-8}	3.1×10^{-8}	1.7×10^{-8}	2.1×10^{-8}	1.9×10^{-8}	5.5×10^{-8}	1.9×10^{-7}	3.8×10^{-7}
C_3H_8	-	-	-	-	1.5×10^{-8}	5.4×10^{-9}			7.6×10^{-9}		1.3×10^{-8}	2.2×10^{-7}	
SF_6	-	-	-	-	7.1×10^{-9}	-	-	-	-	-	4.8×10^{-9}	5.2×10^{-8}	

*Unit of permeance data is mol m^{-2} s^{-1} Pa^{-1}.
-: undetected.

Table S2. Gas permeance from M1 to M13 at 100°C.

Gas	Intrinsic-defects		1 s plasma				2 s plasma
	M1	M3	M5	M6	M9	M11	M12
H_2	4.0×10^{-8}	3.1×10^{-8}	3.8×10^{-7}	2.6×10^{-7}	1.1×10^{-7}	2.9×10^{-7}	6.1×10^{-7}
He	4.9×10^{-8}	1.9×10^{-8}	3.1×10^{-7}	2.2×10^{-7}	1.1×10^{-7}		
CO_2	2.1×10^{-8}	5.2×10^{-9}	1.4×10^{-7}	9.9×10^{-8}	4.6×10^{-8}	1.2×10^{-7}	
CH_4	3.5×10^{-9}	1.7×10^{-9}	4.5×10^{-8}	2.4×10^{-8}	9.6×10^{-9}	2.5×10^{-8}	1.5×10^{-7}
C_3H_8	-	-	3.8×10^{-8}	4.3×10^{-9}	2.4×10^{-9}	1.0×10^{-8}	
SF_6	-	-	9.7×10^{-9}	-	-	-	2.8×10^{-8}

*Unit of permeance data is mol m^{-2} s^{-1} Pa^{-1}.
-: undetected.

Table S3. Gas permeance from M1 to M13 at 30°C.

Gas	Intrinsic-defects		1 s plasma				2 s plasma
	M1	M3	M5	M6	M9	M11	M12
H_2	1.7×10^{-8}	1.3×10^{-8}	1.3×10^{-7}	9.8×10^{-8}	3.6×10^{-8}	7.6×10^{-8}	1.4×10^{-7}
He	1.3×10^{-8}	6.8×10^{-9}	1.0×10^{-7}	7.4×10^{-8}	4.0×10^{-8}		
CO_2	1.4×10^{-8}	2.7×10^{-9}	6.2×10^{-8}	4.6×10^{-8}	2.4×10^{-8}	5.3×10^{-8}	
CH_4	-	-	1.6×10^{-8}	1.3×10^{-8}	6.3×10^{-9}	6.0×10^{-9}	3.6×10^{-8}
C_3H_8	-	-	4.0×10^{-8}	8.5×10^{-9}	3.9×10^{-9}	1.4×10^{-8}	
SF_6	-	-	4.8×10^{-9}	-	-	-	1.8×10^{-8}

*Unit of permeance data is mol m^{-2} s^{-1} Pa^{-1}.
-: undetected.

Table S4. Estimated percentage of large nanopores in graphene after O_2 plasma exposure for different gas molecules.

Graphene	Percentage of pores larger than the kinetic diameter of the gases (ppm)		
	CH_4 (kinetic diameter =0.38 nm)	C_3H_8 (kinetic diameter =0.43 nm)	SF_6 (kinetic diameter =0.55 nm)
Intrinsic-defects	18	-	-
1 s plasma	35	11	9
2 s plasma	141	-	96

*Average selectivity of different samples with the same condition was used in the calculation.

Table S5. Gas permeance from M9 before and after O_3 etching at 60°C for 85 s.

Gas	1 s plasma			1 s plasma + 1 cycle of O_3			1 s plasma + 2 cycles of O_3		
	150 °C	100 °C	30 °C	150 °C	100 °C	30 °C	150 °C	100 °C	30 °C
H_2	2.3×10^{-7}	1.1×10^{-7}	3.6×10^{-8}	4.5×10^{-7}	2.5×10^{-7}	7.7×10^{-8}	7.1×10^{-7}	3.8×10^{-7}	1.1×10^{-7}
He	2.1×10^{-7}	1.1×10^{-7}	4.0×10^{-8}	6.4×10^{-7}	3.2×10^{-7}	9.2×10^{-8}	9.6×10^{-7}	4.8×10^{-7}	1.5×10^{-7}
CO_2	7.5×10^{-8}	4.6×10^{-8}	2.4×10^{-8}	1.9×10^{-7}	1.2×10^{-7}	5.1×10^{-8}	3.0×10^{-7}	2.0×10^{-7}	8.8×10^{-8}
CH_4	2.1×10^{-8}	9.6×10^{-9}	6.3×10^{-9}	2.8×10^{-8}	1.5×10^{-8}	7.1×10^{-9}	4.3×10^{-8}	2.2×10^{-8}	9.8×10^{-9}
C_3H_8	7.6×10^{-9}	2.4×10^{-9}	3.9×10^{-9}	1.4×10^{-8}	8.6×10^{-9}	6.6×10^{-9}	1.9×10^{-8}	8.5×10^{-9}	6.9×10^{-9}

*Unit of permeance data is mol m^{-2} s^{-1} Pa^{-1}.

Table S6. Gas permeance from M7 before and after O_3 etching at 60°C for 85 s.

Gas	1 s plasma	1 s plasma + 1 cycle of O_3		
	150 °C	150 °C	100 °C	30 °C
H_2	2.9×10^{-7}	5.4×10^{-7}	3.3×10^{-7}	1.2×10^{-7}
He		5.5×10^{-7}	2.7×10^{-7}	9.9×10^{-8}
CO_2		1.7×10^{-7}	1.2×10^{-7}	7.2×10^{-8}
CH_4	3.1×10^{-8}	4.8×10^{-8}	2.4×10^{-8}	1.4×10^{-8}

*Unit of permeance data is mol m^{-2} s^{-1} Pa^{-1}.

Table S7. Gas permeance from M10 before and after O_3 etching at 150°C for 10 s.

Gas	1 s plasma	1 s plasma + 1 cycle of O_3		
	150 °C	150 °C	100 °C	30 °C
H_2	2.4×10^{-7}	2.1×10^{-6}	1.1×10^{-6}	3.7×10^{-7}
He		2.8×10^{-6}	1.5×10^{-6}	4.5×10^{-7}
CO_2		8.2×10^{-7}	5.3×10^{-7}	2.7×10^{-7}
CH_4	1.9×10^{-8}	1.3×10^{-7}	8.1×10^{-8}	3.4×10^{-8}
SF_6	-	1.3×10^{-8}	2.0×10^{-8}	1.3×10^{-8}

*Unit of permeance data is mol m^{-2} s^{-1} Pa^{-1}.
-: undetected.

Table S8. Percentage of nanopores larger than 0.38 nm after post cycles of O_3 etching.

Graphene used	O_3 treatment cycles	ppm of pores larger than the kinetic diameter of CH_4 (0.38 nm)			
		Cycle 0	Cycle 1	Cycle 2	Cycle 3
M2 (intrinsic-defects)	150 °C for 10 s for 3 cycles	15	10	11	30
M4 (intrinsic-defects)	Cycle 1: 25 °C for 85 s Cycles 2 and 3: 150 °C for 10 s	13	8	13	60
M7 (1 s plasma)	60 °C for 85 s	43	29		
M9 (1 s plasma)	60 °C for 85 s for 2 cycles	35	21	21	
M10 (1 s plasma)	150 °C for 10 s	28	22		

Cycle 0: Graphene before O_3 treatment (performance from the intrinsic-defects or the pores generated by plasma)
Cycle 1: Graphene after one-cycle of O_3 treatment
Cycle 2: Graphene after two-cycles of O_3 treatment
Cycle 3: Graphene after three-cycles of O_3 treatment

Table S9. Gas permeance from M2 before and after O_3 etching at 150°C for 10 s.

Gas	Intrinsic-defects	1st cycle of O_3, 150 °C for 10 s			2nd cycle of O_3, 150 °C for 10 s	3rd cycle of O_3, 150 °C for 10 s
	150 °C	150 °C	100 °C	30 °C	150 °C	150 °C
H_2	5.5×10^{-8}	8.8×10^{-7}	5.4×10^{-7}	1.5×10^{-7}	1.0×10^{-6}	1.3×10^{-6}
He	4.7×10^{-8}	1.2×10^{-6}	6.2×10^{-7}	1.8×10^{-7}		
CO_2	1.5×10^{-8}	2.3×10^{-7}	1.7×10^{-7}	8.0×10^{-8}		
CH_4	2.6×10^{-9}	2.9×10^{-8}	1.4×10^{-8}	2.8×10^{-9}	3.6×10^{-8}	1.1×10^{-7}
C_3H_8	-	4.2×10^{-9}	-	-	7.1×10^{-9}	1.1×10^{-7}

*Unit of permeance data is mol m^{-2} s^{-1} Pa^{-1}.
-: undetected.

Table S10. Gas permeance from M4 before and after O_3 etching.

Gas	Intrinsic-defects	O_3, 25 °C for 120 s	1st cycle of O_3, 150 °C for 10 s			2nd cycle of O_3, 150 °C for 10 s
	150 °C	150 °C	150 °C	100 °C	30 °C	150 °C
H_2	9.1×10^{-8}	6.6×10^{-8}	1.2×10^{-6}	7.0×10^{-7}	2.5×10^{-7}	3.7×10^{-6}
He	8.9×10^{-8}	7.6×10^{-8}	1.5×10^{-6}	8.2×10^{-7}	2.9×10^{-7}	
CO_2	2.5×10^{-8}	1.4×10^{-8}	3.4×10^{-7}	2.6×10^{-7}	1.6×10^{-7}	
CH_4	3.9×10^{-9}	1.7×10^{-9}	4.6×10^{-8}	2.6×10^{-8}	7.1×10^{-9}	4.9×10^{-7}
C_3H_8	-	-	2.0×10^{-8}	1.5×10^{-8}	8.2×10^{-9}	5.8×10^{-7}

*Unit of permeance data is mol m^{-2} s^{-1} Pa^{-1}.
-: undetected.

Table S11. Comparison of H_2/CH_4 separation performance in this work with that in other literatures.

Membrane	H_2 Permeance ($\times10^{-8}$ mol m^{-2} s^{-1} Pa^{-1})	H_2 Permeance (GPU)	SF (H_2/CH_4)	Reference
Our work on Graphene membrane				
1 s plasma + 150 °C O_3 [a]	205	6045	15.6	This work
150 °C O_3 (2 cycles) [a]	104	3071	29.0	This work
25 °C O_3 + 150 °C O_3 [a]	115	3400	25.1	This work
25 °C O_3 + 150 °C O_3 (2 cycles) [a]	368	10833	7.5	This work
Graphene				
Single-layer graphene[a]	45	1326	17	(*5*)
Single-layer graphene[a]	21	619	20	(*5*)
Zeolite				
AIPO-18	10	300	22	(*43*)
SSZ-13	8	236	7	(*33*)
Natural zeolite	3	94	6.5	(*44*)
FAU	19	566	9.9	(*34*)
MOF				
ZIF-8/GO	13	383	139	(*45*)
ZIF-90	25	740	15.3	(*46*)
$Cu_3(BTC)_2$	198	5830	5.9	(*47*)
ZIF-7-8	17	510	7.5	(*48*)
ZIF-67	16	461	41.9	(*49*)
JCU-150	18	533	26.3	(*31*)

NH_2-MIL-53(Al)	152	4471	20.7	(*32*)
GO				
GO/AAO	11	309	117	(*36*)
GO-thiourea[b]	20	589	66.7	(*35*)
CMS				
CMS/TiO_2-Al_2O_3[c]	5.7	167	726	(*37*)
CMS/Al_2O_3[d]	18.6	548	35	(*50*)
CMS/Al_2O_3[c]	11.9	350	160	(*51*)

[a] These data are from single-gas test under pressure difference of 2 bar at 150 °C.
[b] These data are from single-gas test under pressure difference of 1 bar at 25 °C.
[c] These data are from single-gas test under pressure difference of 2 bar at 25 °C.
[d] These data are from single-gas test under pressure difference of 3 bar at 120 °C.

Table S12. Gas permeance from M14 (1-s plasma-treated membrane) before and after 150°C treatment used to remove contaminants.

Temperature	H_2 permeance	H_2/CH_4 selectivity
30 ^oC (before heating)	56 GPU	5.9
150 ^oC	705 GPU	8.9
30 ^oC (after heating)	216 GPU	7.3